# Supporting Information

## High-stable Mn-based cathode with low crystalline $Li_2MnO_3$ and spinel functional units for lithium-ion batteries

Shiqi Liu‡[a,b,f], Yinzhong Wang‡[a,b,e], Dongdong Xiao‡[c], Haifeng Li[a,b], Tianhao Wu[a,b], Boya Wang[a,b], Guangxing Hu[a,b], Lingqiao Wu [a,b], Yulong Wang[a,b], Guoqing Wang[a,b,e], Nian Zhang[d] and Haijun Yu[a,b,f,*]

[a]Institute of Advanced Battery Materials and Devices, College of Materials Science and Engineering, Beijing University of Technology, Beijing 100124, China. E-mail: hj-yu@bjut.edu.cn

[b]Key Laboratory of Advanced Functional Materials, Ministry of Education, Beijing University of Technology, Beijing 100124, China.

[c]Beijing National Laboratory for Condensed Matter Physics, Institute of Physics, Chinese Academy of Sciences, Beijing 100190, China.

[d]State Key Laboratory of Functional Materials for Informatics, Shanghai Institute of Microsystem and Information Technology, Chinese Academy of Sciences, Shanghai 200050, People's Republic of China.

[e]Beijing Create Energy & Benefit Future Co., Ltd., Beijing 100176, China.

[f]Institute of Matter Science, Beijing University of Technology, Beijing 100124, China.

‡These authors contributed equally to this work.

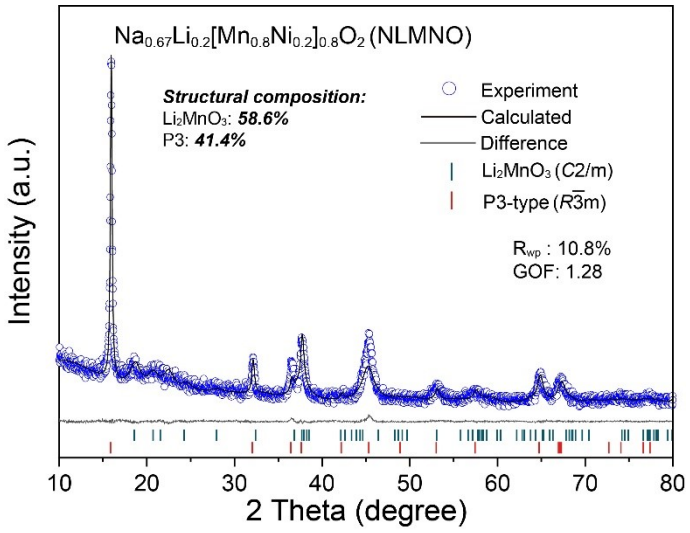


**Figure S1.** XRD refinement of NLMNO.

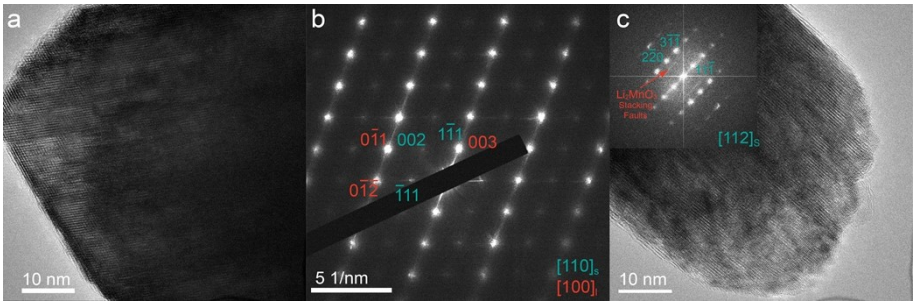


**Figure S2.** TEM images and corresponding SAED and FFT patterns of PHS-LLMNO within different particles.

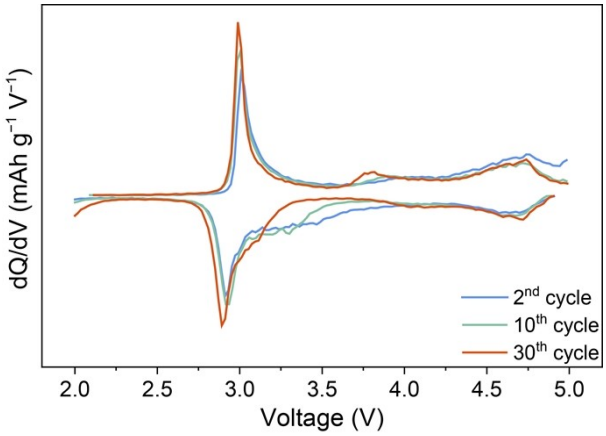


**Figure S3.** The dQ/dV curves of PHS-LLMNO in different cycles at 10 mA $g^{-1}$.

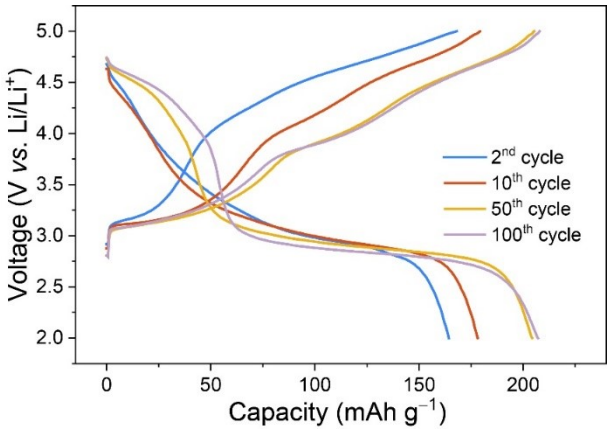


**Figure S4.** Charge/discharge profiles of PHS-LLMNO in different cycles at 200 mA $g^{-1}$.

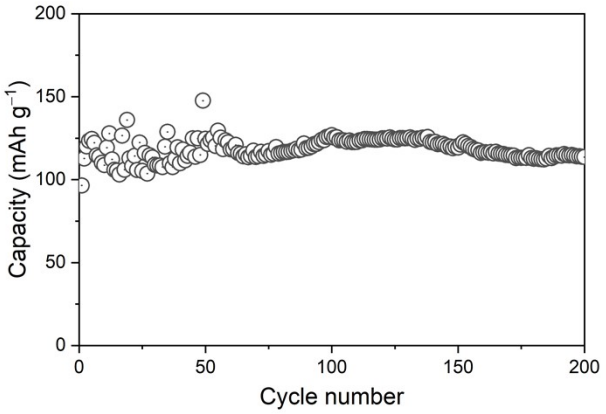


**Figure S5.** The capacity retention of PHS-LLMNO with the high mass loading of active material of 6.5 mg cm$^{-2}$ at 600 mA g$^{-1}$.

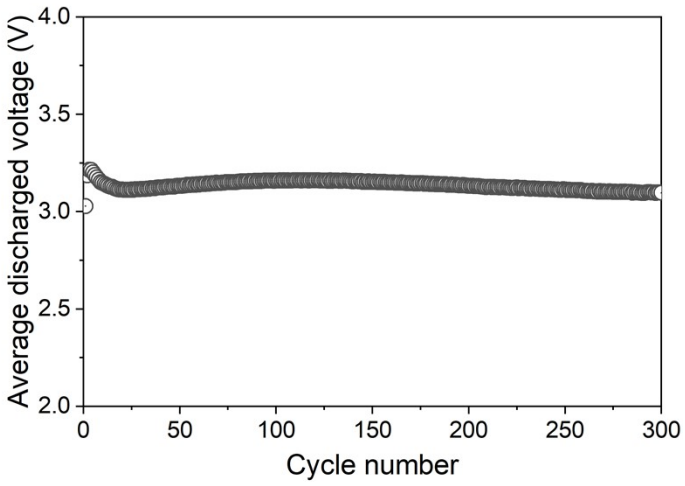


**Figure S6.** The variation of average discharged voltage versus cycle number at 300 mA $g^{-1}$.

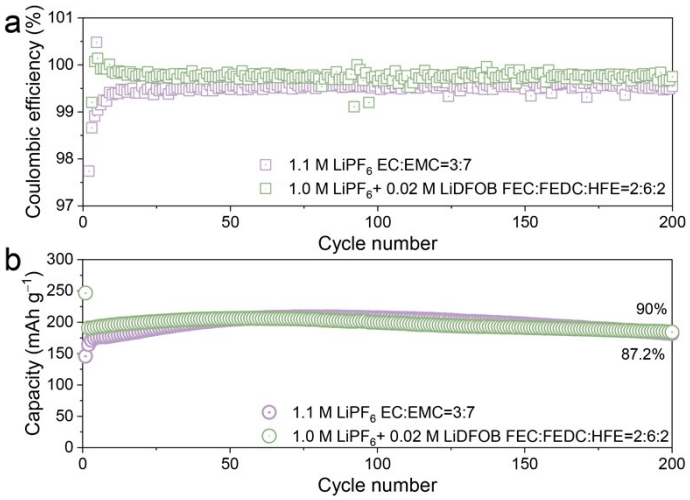


**Figure S7.** (a) Coulombic efficiency and (b) capacity retention of PHS-LLMNO in different electrolytes at 200 mA $g^{-1}$.

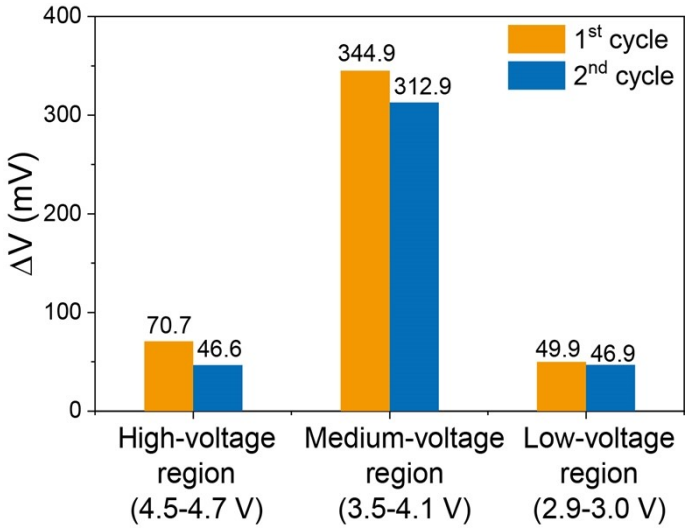


**Figure S8.** The calculated overpotentionals at selected voltage regions upon the discharge processes of the initial two cycles under GITT measurement.

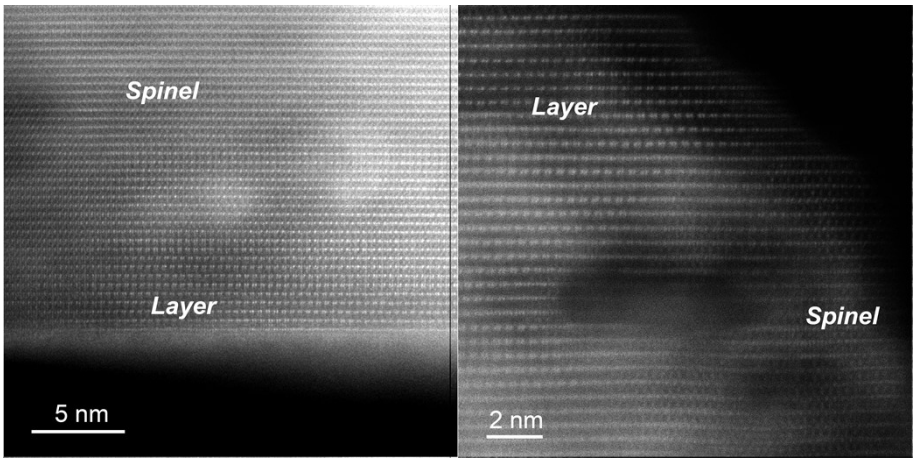


**Figure S9.** HAADF–STEM images of PHS-LLMNO in different particles and areas.

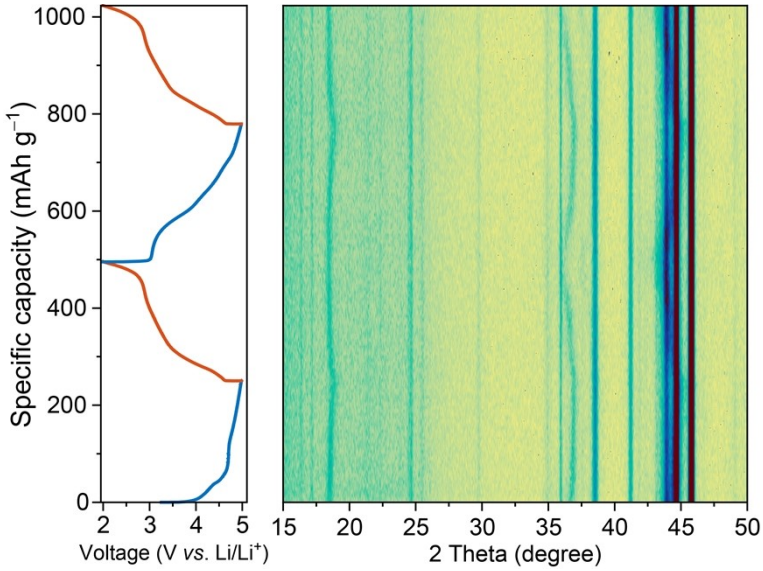


**Figure S10.** The *in situ* XRD 2D contour image and corresponding charge/discharge profiles of PHS-LLMNO.

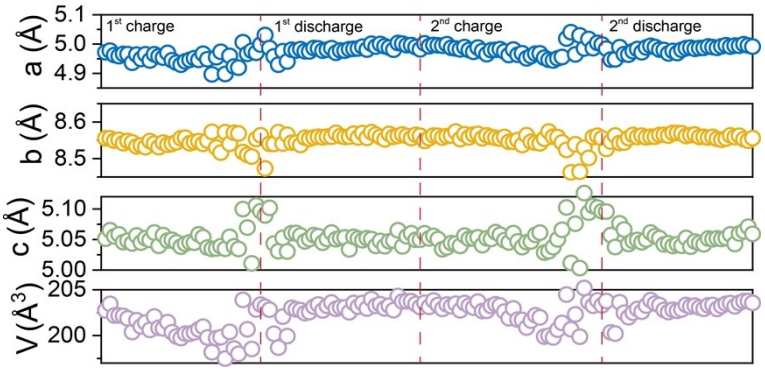


**Figure S11.** Variation of cell parameters a, b, c and V in the initial two cycles of PHS-LLMNO, respectively.

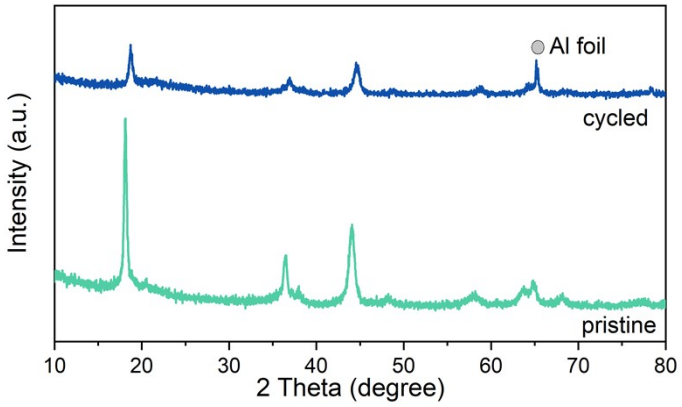


**Figure S12.** XRD pattern of PHS-LLMNO cathode before and after cycling.

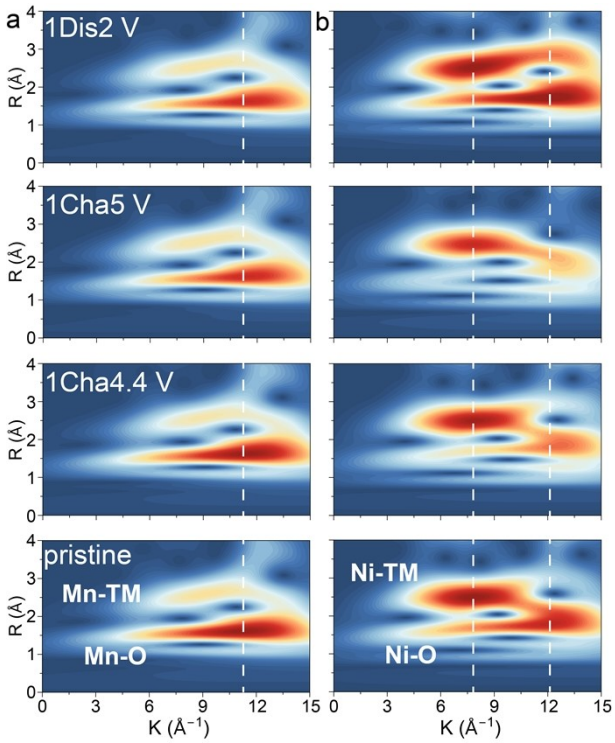


**Figure S13.** Wavelet transforms of (a) Mn *K*-edge and (b) Ni *K*-edge EXAFS spectra in PHS-LLMNO at different electrochemical states.

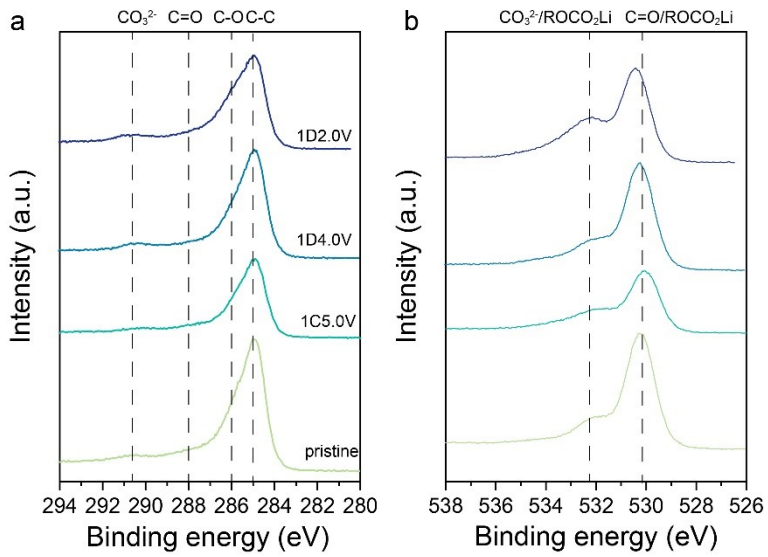


**Figure S14.** The ex situ XPS (a) C1s and (b) F1s spectra of PHS-LLMNO at the pristine, charged to 5.0 V, discharged to 4.0 V and discharged to 2.0 V, respectively.

**Table S1**. Stoichiometry from Inductively coupled plasma (ICP) results of PHS-LLMNO.

| Elements | content (mg/L) | molar ratio |
|---|---|---|
| Li | 11.9 | 0.80 |
| Mn | 75.1 | 0.64 |
| Ni | 20.3 | 0.16 |

**Table S2.** XRD refinement results of PHS-LLMNO based on two-phase model of monoclinic *C2*/m space group of $Li_2MnO_3$ and cubic $P4_332$ space group of $LiMn_{1.5}Ni_{0.5}O_4$.

| Site | Wyckoff position | *x* | *y* | *z* |
|---|---|---|---|---|
| Mn1 | 4g | 0 | 0.172(3) | 0 |
| Li1 | 4g | 0 | 0.172(3) | 0 |
| Li2 | 2b | 0 | 0.5 | 0 |
| Mn2 | 2b | 0 | 0.5 | 0 |
| Li3 | 2c | 0 | 0 | 0.5 |
| Li4 | 4h | 0 | 0.69120 | 0.5 |
| O1 | 4i | 0.240(1) | 0 | 0.246(1) |
| O2 | 8j | 0.249(6) | 0.336(5) | 0.221(5) |
| Phase $Li_2MnO_3$, a=4.953(5) Å; b=8.589(9) Å; c=5.067(2) Å; β=109.640(1)°V = 203.06(8) Å$^3$, fraction: 69.16(3) % | | | | |
| Site | Wyckoff position | *x* | *y* | *z* |
| Li | 8c | 0.00373 | 0.00373 | 0.00373 |
| Mn | 12b | 0.12118 | 0.12882 | 0.62500 |
| Ni | 4b | 0.12500 | 0.87500 | 0.37500 |
| O1 | 24e | 0.195(5) | 0.004(8) | 0.002(7) |
| O2 | 8c | 0.11553 | 0.61553 | 0.88447 |
| Phase $LiMn_{1.5}Ni_{0.5}O_4$, a = 8.162(8) Å; V = 543.738(2) Å$^3$, fraction: 30.84(1) % | | | | |